Boundaryless finite-difference method for three-dimensional beam propagation

Manuel Guizar-Sicairos and Julio C. Gutiérrez-Vega

Photonics and Mathematical Optics Group, Tecnológico de Monterrey, Monterrey, México, 64849

Received July 8, 2005; revised October 14, 2005; accepted October 20, 2005; posted October 25, 2005 (Doc. ID 63332)

A two-dimensional optical field paraxial propagation scheme, in Cartesian and cylindrical coordinate systems, is proposed. This is achieved by extending the method originally proposed by Ladouceur [Opt. Lett. **21**, 4 (1996)] for boundaryless beam propagation to two-dimensional optical wave fields. With this formulation the arbitrary choice of physical window size is avoided by mapping the infinite transverse dimensions into a finite-size domain with an appropriate change of variables, thus avoiding the energy loss through the artificial physical boundary that is usually required for the absorbing or the transparent boundary approach. © 2006 Optical Society of America

OCIS codes: 350.5500, 000.4430, 050.1960.

1. INTRODUCTION

Since the introduction of the original beam propagation method by Feit and Fleck,[1] many extensions and improvements have been proposed. In attempting to numerically analyze the propagation of a two-dimensional wave field, a finite computational window is required in the transverse plane. This limitation imposes an artificial boundary condition on the problem that leads to nonphysical reflections of outgoing waves into the solution region and produces undesired interference with the propagating wave field.

The most common way to prevent this boundary reflection has been the insertion of an artificial absorbing region adjacent to the computational window boundaries.[2] This procedure commonly leads to accurate results, provided that the absorption gradient is small enough to prevent the absorber itself from generating reflections and has a sufficient thickness to absorb all outgoing radiation.

Another approach to solve this problem consists of the introduction of a transparent boundary condition that allows radiation to escape the problem freely without appreciable reflection into the region of interest. This approach was first proposed by Hadley[3] for finite-difference analysis and later extended to finite-element analysis by Arai *et al.*[4]

These two commonly used techniques allow energy and information to escape or be reduced in the computational window and may not be useful if the field region of interest is continuously expanding in the transverse direction. To prevent this problem and the arbitrary choice of a large enough simulation window, Ladouceur proposed the mapping of the infinite one-dimensional transverse coordinates to a finite-size domain and numerically solved the modified propagation equation.[5] Shibayama *et al.* later applied this mapping technique to the wide-angle formulation.[6]

In this paper we extend the propagation scheme proposed by Ladouceur for the scalar regime to two transverse dimensions in Cartesian and cylindrical coordinate systems. We apply the new formulations to propagate sample wave fields and compare the results with their analytic solutions. A discussion of the method limitations due to the continuously growing sampling step is also given.

2. CARTESIAN COORDINATE SYSTEM

In the weak-guidance regime, the polarization of the field can be assumed to be linear, and the paraxial approximation of the scalar Helmholtz equation may be used. In Cartesian coordinates this equation is given by[5]

$$\frac{\partial^2 U(\mathbf{r},z)}{\partial x^2}+\frac{\partial^2 U(\mathbf{r},z)}{\partial y^2}+2i\bar{k}\frac{\partial U(\mathbf{r},z)}{\partial z}+[k^2-\bar{k}^2]U(\mathbf{r},z)=0, \tag{1}$$

where the scalar electric field is

$$E(\mathbf{r},z)=U(\mathbf{r},z)\exp(i\bar{k}z), \tag{2}$$

where $\bar{k}$ is the average wavenumber, $k=k(\mathbf{r},z)$ is the local wavenumber related to an arbitrary distribution of refractive index, $\mathbf{r}$ is the transverse set of coordinates (x,y), and z is the axis of propagation.

To avoid limitation of the solution region by the computational window when numerically solving Eq. (1), we map the infinite x and y dimensions onto a finite square domain through the mapping functions

$$x=\alpha\tan u, \tag{3a}$$

$$y=\beta\tan v, \tag{3b}$$

where α and β are independent scaling parameters that conveniently allow us to control the sampling of the propagating function. The new variables (u,v) have a range of $[-\pi/2,\pi/2]$. The sampling interval in the physical space increases gradually from the center to the edge of the computational window; this mapping is particularly

suitable for representation of optical waveguide modes and has been previously applied to waveguide eigenmode analysis.[7,8] This occurs because the region with high-field amplitude is densely discretized, and low-field amplitude regions are scarcely discretized.

After substituting the mapping functions in Eqs. (3) into Eq. (1), we apply a simple field transformation,

$$U(u,v,z) = \frac{\psi(u,v,z)}{\cos u \cos v}, \tag{4}$$

in order to eliminate the first derivative of the field with respect to the transverse coordinates and simplify the resulting equation. Equation (1) yields

$$\frac{\cos^4 u}{\alpha^2}\frac{\partial^2\psi}{\partial u^2} + \frac{\cos^4 v}{\beta^2}\frac{\partial^2\psi}{\partial v^2} + \left[k^2 - \bar{k}^2 + \frac{\cos^4 u}{\alpha^2} + \frac{\cos^4 v}{\beta^2}\right]\psi + 2i\bar{k}\frac{\partial\psi}{\partial z} = 0. \tag{5}$$

Equation (5) can be numerically solved using the known alternating direction implicit method in two dimensions.[9]

We define Δu and Δv as the sampling intervals in the u and v transverse space, respectively, Δz as the propagation step,

$$u_p \equiv p\Delta u, \qquad p = 0,1,\ldots,N_u - 1, \tag{6a}$$

$$v_j \equiv j\Delta v, \qquad j = 0,1,\ldots,N_v - 1, \tag{6b}$$

$$\psi_{p,j}^{(m)} \equiv \psi(u_p, v_j, m\Delta z), \qquad m = 0,1,2,\ldots. \tag{6c}$$

By discretizing Eq. (5) around an intermediate step $z = (m+1/2)\Delta z$ using the alternating direction implicit method, we obtain the finite-difference equations

$$\frac{2i\bar{k}}{\Delta z/2}[\psi_{p,j}^{(m+1/2)} - \psi_{p,j}^{(m)}] + \frac{\cos^4 u_p}{\Delta u^2\alpha^2}[\psi_{p+1,j}^{(m+1/2)} - 2\psi_{p,j}^{(m+1/2)} + \psi_{p-1,j}^{(m+1/2)}] + \frac{\cos^4 v_j}{\Delta v^2\beta^2}[\psi_{p,j+1}^{(m)} - 2\psi_{p,j}^{(m)} + \psi_{p,j-1}^{(m)}] + \left[\frac{\cos^4 u_p}{\alpha^2} - \frac{\bar{k}^2}{2}\right]\psi_{p,j}^{(m+1/2)} + \left[\frac{\cos^4 v_j}{\beta^2} - \frac{\bar{k}^2}{2}\right]\psi_{p,j}^{(m)} = 0, \tag{7a}$$

$$\frac{2i\bar{k}}{\Delta z/2}[\psi_{p,j}^{(m+1)} - \psi_{p,j}^{(m+1/2)}] + \frac{\cos^4 u_p}{\Delta u^2\alpha^2}[\psi_{p+1,j}^{(m+1/2)} - 2\psi_{p,j}^{(m+1/2)} + \psi_{p-1,j}^{(m+1/2)}] + \frac{\cos^4 v_j}{\Delta v^2\beta^2}[\psi_{p,j+1}^{(m+1)} - 2\psi_{p,j}^{(m+1)} + \psi_{p,j-1}^{(m+1)}] + \left[\frac{\cos^4 u_p}{\alpha^2} - \frac{\bar{k}^2}{2}\right]\psi_{p,j}^{(m+1/2)} + \left[\frac{\cos^4 v_j}{\beta^2} - \frac{\bar{k}^2}{2}\right]\psi_{p,j}^{(m+1)} + 2(k_{p,j}^{(m+1/2)})^2\psi_{p,j}^{(m+1/2)} = 0, \tag{7b}$$

where we preserve generality in the refractive index three-dimensional dependence by means of the wavenumber $k_{p,j}^{(m+1/2)} \equiv k(u_p, v_j, (m+1/2)\Delta z)$.

Notice that the contribution of the wavenumber $k_{p,j}^{(m+1/2)}$ is considered only in Eq. (7b). We do this to be able to rewrite Eq. (7a) in terms of matrix multiplications, since the local wavenumber requires an element-by-element multiplication with $\psi_{p,j}$. With this expression we are able to solve for $\psi_{p,j}^{(m+1/2)}$ in Eq. (7a) in terms of matrix multiplication operations, and we minimize the required operations in each propagation step. Although this breaks the expected symmetry, it greatly reduces the computation time of the method.

It is straightforward to show that expressions (7) can be rearranged as

$$\left[\frac{4i\bar{k}}{\Delta z} + b_p\right]\psi_{p,j}^{(m+1/2)} + a_p[\psi_{p+1,j}^{(m+1/2)} + \psi_{p-1,j}^{(m+1/2)}] = \left[\frac{4i\bar{k}}{\Delta z} - d_j\right]\psi_{p,j}^{(m)} - c_j[\psi_{p,j+1}^{(m)} + \psi_{p,j-1}^{(m)}], \tag{8a}$$

$$\left[\frac{4i\bar{k}}{\Delta z} + d_j\right]\psi_{p,j}^{(m+1)} + c_j[\psi_{p,j+1}^{(m+1)} + \psi_{p,j-1}^{(m+1)}] = \left[\frac{4i\bar{k}}{\Delta z} - b_p - 2(k_{p,j}^{(m+1/2)})^2\right]\psi_{p,j}^{(m+1/2)} - a_p[\psi_{p+1,j}^{(m+1/2)} + \psi_{p-1,j}^{(m+1/2)}], \tag{8b}$$

where we have defined

$$a_p \equiv \frac{\cos^4 u_p}{\Delta u^2\alpha^2}, \tag{9a}$$

$$b_p \equiv a_p(\Delta u^2 - 2) - \frac{\bar{k}^2}{2}, \tag{9b}$$

$$c_j \equiv \frac{\cos^4 v_j}{\Delta v^2\beta^2}, \tag{9c}$$

$$d_j \equiv c_j(\Delta v^2 - 2) - \frac{\bar{k}^2}{2}. \tag{9d}$$

Equations (8) can be solved efficiently by expressing them in matrix multiplication and array element-by-element multiplication; in this format we do not need to explicitly compute the intermediate function $\psi_{p,j}^{(m+1/2)}$. The inverse of matrices is computed only once in this approach, and only the array $k_{p,j}^{(m+1/2)}$ is modified to account for longitudinal dependence of the refractive index.

In the particular case where the square of the refractive index is longitudinally constant and can be expressed as a sum of horizontal and vertical contributions, namely, $k^2(u,v,z) = k_x^2(u) + k_y^2(v)$, the finite-difference equations, Eqs. (7), may be restated in a more efficient form that involves only matrix products. In this case the wavenumber contribution should appear in Eqs. (8a) and (8b) in both sides of the equalities and may be included in the definitions of b_p and d_j.

3. NUMERICAL TEST IN CARTESIAN COORDINATES

To test the proposed algorithm, we propagate a cosine-Gauss beam in free space; cosine-Gauss fields are a special case of the Helmholtz–Gauss beams[10] whose analytical exact propagation equation is known.

The field of a cosine-Gauss beam at a distance $z=0$, as depicted in Fig. 1(a), is given by

$$U(\mathbf{r},0)=\exp\left(-\frac{r^2}{w_0^2}\right)\cos(k_t x), \tag{10}$$

where r is the radial coordinate, $w_0=1$ mm is the spot waist, $k_t=8\times10^{-4}\bar{k}$ is the field transverse wavenumber, and an illumination of $\lambda=632.8$ nm is assumed. The complete (u,v) space is sampled with $N_u=1501$ and $N_v=301$ points in the u space and v space, respectively, and mapping parameters $\alpha=20$ mm and $\beta=10$ mm are implemented. The difference boundary condition at plane $z=0$ corresponding to Eq. (10) is written explicitly as

$$\psi_{p,j}^{(0)}=\exp\left(-\frac{x_p^2+y_j^2}{w_0^2}\right)\cos(k_t x_p)\cos u_p \cos v_j, \tag{11}$$

where $x_p=\alpha\tan u_p$ and $y_j=\beta\tan v_j$.

A comparison between the propagation of the cosine-Gauss beam computed with the proposed algorithm and the analytical function[10] is depicted in Fig. 1(b). Notice that a fairly good agreement is achieved. Figure 1(c) shows the propagating field intensity along the (x,z) plane; this field behaves like a nondiffracting cosine field within the range $z\leqslant w_0\bar{k}/k_t\simeq1.25$ m.

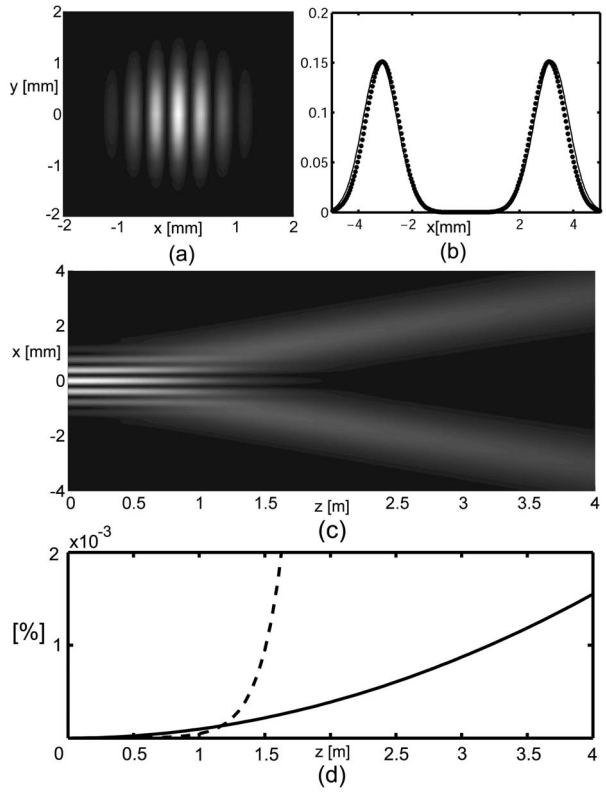

Fig. 1. (a) Cosine-Gauss field intensity at $z=0$. (b) Comparison between analytical cosine-Gauss field intensity at $z=4$ m (solid curve) and that obtained with the proposed algorithm (dots). (c) Propagating field intensity in the (x,z) plane. (d) Percentage error of computed energy as a function of the propagated distance for the proposed algorithm (solid curve) and a typical absorbing boundary method (dashed curve).

A clear advantage of this method over the absorbing boundary method and the transparent window approach is that simulation stability can be monitored with the computation of the percentage error of the energy in each propagation step, namely,

$$e(z)=\frac{|\Omega(z)-\Omega_0|}{\Omega_0}(100\,\%), \tag{12}$$

where $\Omega(z)$ is the field energy computed at each propagation step and Ω_0 is the analytically obtained energy of the input field. Since the sampling intervals are not constant, integration was performed using a two-dimensional trapezoidal approach. Figure 1(d) shows (solid curve) the computed percentage error of the energy for the cosine-Gauss beam propagation.

For a comparison with the absorbing boundary method, we implemented also a standard two-dimensional propagator based on the angular spectrum representation of plane waves utilizing the fast Fourier transform algorithm. The transverse field was sampled in the transverse domain $[|x|<6,|y|<6]$ mm over a grid of 512×512 points, and the absorber was implemented using a typical super-Gaussian function $\exp[-(r/w)^{20}]$ with $w=5$ mm. Figure 1(d) shows (dashed curve) the percentage error of the energy using the absorber method. As expected, once the field energy reaches the computational boundary, the error increases dramatically.

We found that, in general, the implemented mapping is not particularly suitable to represent tilted wave fields, as the cosine-Gauss beam may be regarded as the sum of two tilted Gaussian beams. Tilted beams tend to have high-field magnitude moving outward in the physical space into the scarcely sampled regions. The subsampled tilted field suffers from frequency aliasing and tends to return to the central region of the computational window. The maximum sampling period to avoid tilt phase aliasing is given by $x_{p+1}-x_p=\pi/k_t$, using the definition of the discretized physical coordinate $x_p=\alpha\tan u_p$ and Eqs. (6). It is straightforward to show that the limiting sampling condition can be expressed as

$$\cos[(2p+1)\Delta u]=\frac{2\alpha k_t\sin\Delta u}{\pi}-\cos\Delta u. \tag{13}$$

In the implemented numerical example, the index condition to avoid tilt phase aliasing computed from expression (13) is $p\leqslant613$; this corresponds to a propagation limit in the physical space $|x|\leqslant x_{p=613}\simeq58.7$ mm. Any field energy propagating beyond this transverse position will experience frequency aliasing; thus adequate sampling should be a primary matter of concern when this algorithm is applied. In the example, the computational requirements for the horizontal sampling are greater than those of the vertical sampling to ensure that the field is properly discretized as it moves outward in the transverse coordinate.

Exclusive consideration of tilt frequency is an optimistic approach of the method sampling limitations. In this case we retrieve the transverse position where aliasing will surely occur because a tilted wave field always contains frequencies beyond that of the tilt phase profile. To delimit the transverse area where an arbitrary signal will be accurately represented, we should replace the tilt spatial frequency k_t in Eq. (13) with the actual bandwidth of the wave field and perform an equivalent analysis in the y coordinate.

Although the proposed method is not especially suitable for propagating tilted wave fields, good results can be observed in the comparison with the analytical function; see Fig. 1(b). Other tests performed with nontilted high-order Laguerre–Gauss and Hermite–Gauss beams have provided better results for propagation distances larger than $z=15$ m with a 301×301 grid. As these fields propagate, they slowly enter some scarcely sampled regions of the physical space, but also the sampling requirements are continuously relaxed owing to diffraction.

4. CYLINDRICAL COORDINATE SYSTEM

In cylindrical coordinates, the paraxial approximation of the scalar Helmholtz equation, Eq. (1), is given by

$$\frac{1}{r}\frac{\partial}{\partial r}\left[r\frac{\partial f(r,z)}{\partial r}\right]+2i\bar{k}\frac{\partial f(r,z)}{\partial z}+\left[k^2-\bar{k}^2-\frac{l^2}{r^2}\right]f(r,z)=0, \tag{14}$$

where (r,ϕ) are the set of transverse cylindrical coordinates and we have assumed some order of azimuthal symmetry in the field, namely,

$$U(\mathbf{r},z)=f(r,z)\exp(il\phi). \tag{15}$$

We map the radial coordinate r of infinite range $(0,\infty)$ to a variable ρ of finite range $(0,\pi/2]$, through the mapping function

$$r=\gamma\tan\rho, \tag{16}$$

where γ is the coordinate scaling parameter that allows us to control the sampling. Substitution of Eq. (16) into Eq. (14) yields

$$\frac{\cos^4\rho}{\gamma^2}\frac{\partial^2 f}{\partial\rho^2}+\frac{\cos^3\rho}{\gamma^2\sin\rho}[2\cos^2\rho-1]\frac{\partial f}{\partial\rho}+2i\bar{k}\frac{\partial f}{\partial z}+\left[k^2-\bar{k}^2-\frac{l^2}{\gamma^2\tan^2\rho}\right]f=0. \tag{17}$$

We found a field transformation, analogous to Eq. (4), that eliminates the first derivative of the field with respect to the mapped radial coordinate ρ, thus simplifying the resulting difference equation. However, this field transformation requires an infinite boundary condition at $\rho=0$ and compromises stability of the numerical simulation. Therefore we omit this field transformation and simply derive the finite-difference equation from Eq. (17) using the Crank–Nicolson method.[9]

We discretize the radial mapped coordinate ρ in the range $(0,\pi/2]$ with $\Delta\rho$ as the sampling interval and Δz as the propagation step. Defining $\rho_p=p\Delta\rho$, with $p=0,1,\ldots,N_\rho-1$, and $f_p^{(m)}\equiv f(\rho_p,m\Delta z)$, we find that the resulting difference equation is

$$\left[\frac{2i\bar{k}}{\Delta z}+a_p\right]f_p^{(m+1)}+b_p f_{p+1}^{(m+1)}+c_p f_{p-1}^{(m+1)}=\left[\frac{2i\bar{k}}{\Delta z}-a_p\right]f_p^{(m)}-b_p f_{p+1}^{(m)}-c_p f_{p-1}^{(m)}, \tag{18}$$

where

$$a_p\equiv\frac{1}{2}\left[(k_p^{(m+1/2)})^2-\bar{k}^2-\frac{l^2}{\gamma^2\tan^2\rho_p}\right]-\frac{\cos^4\rho_p}{\gamma^2\Delta\rho^2}, \tag{19a}$$

$$b_p\equiv\frac{\cos^4\rho_p}{2\gamma^2\Delta\rho^2}+\frac{\cos^3\rho_p}{4\gamma^2\Delta\rho\sin\rho_p}[2\cos^2\rho_p-1], \tag{19b}$$

$$c_p\equiv\frac{\cos^4\rho_p}{2\gamma^2\Delta\rho^2}-\frac{\cos^3\rho_p}{4\gamma^2\Delta\rho\sin\rho_p}[2\cos^2\rho_p-1], \tag{19c}$$

$$k_p^{(m)}\equiv k(\rho_p,m\Delta z). \tag{20}$$

Equation (18) can be solved using any tridiagonal solver. In this approach, longitudinal variation of the refractive index distribution is allowed through the discretized wavenumber $k_p^{(m)}$; however, this formulation is limited to radial variations and cannot account for azimuthal dependence of the refractive index.

5. NUMERICAL TEST IN CYLINDRICAL COORDINATES

The propagation in free space of a Bessel–Gauss beam is implemented to test the accuracy of the proposed algorithm. As another special case of the Helmholtz–Gauss beams,[10] the analytical expression of the propagated wave field is known and may be compared with the numerical results.

The transverse field of the lth-order Bessel–Gauss beam at $z=0$ reads as

$$U(\mathbf{r},0)=J_l(k_t r)\exp(il\phi)\exp\left(-\frac{r^2}{w_0^2}\right), \tag{21}$$

where $J_l(\cdot)$ is the lth-order Bessel function of the first kind. We take the beam waist $w_0=1$ mm and assume an illumination at wavelength $\lambda=632.8$ nm, a transverse wavenumber of $k_t=8\times10^{-4}\bar{k}$, an azimuthal order of the propagated field $l=3$, and $\gamma=3$ mm. Figure 2(a) depicts the field radial intensity profile of the Bessel–Gauss beam at $z=0$. The difference boundary condition at plane $z=0$ corresponding to Eq. (21) is written explicitly as

$$f_p^{(0)}=J_l(k_t\gamma\tan\rho_p)\exp\left(-\frac{\gamma^2\tan^2\rho_p}{w_0^2}\right). \tag{22}$$

A radial intensity profile comparison of the numerically propagated wave field with the analytic function for

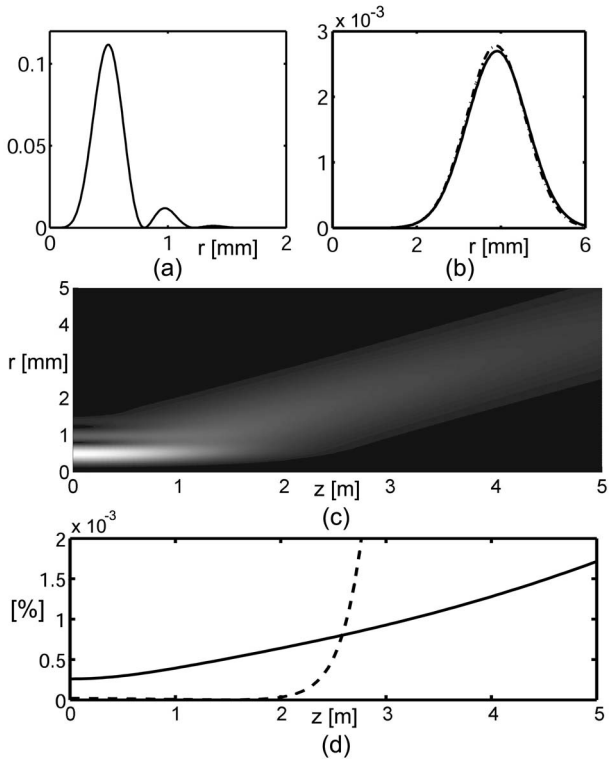

Fig. 2. (a) Bessel–Gauss field intensity at $z=0$. (b) Comparison between an analytical Bessel–Gauss field at $z=5$ m (solid curve) and that obtained with the proposed algorithm (dashed–dotted curve). (c) Propagating field intensity in the (r,z) plane. (d) Percentage error of computed energy as a function of the propagated distance for the proposed algorithm (solid curve) and a typical absorbing boundary method (dashed curve).

$z=5$ m is provided in Fig. 2(b). The propagated field intensity in the (r,z) plane is shown in Fig. 2(c), as a special case of the Helmholtz–Gauss beams; this field behaves like a nondiffracting third-order Bessel beam within the range $z \leqslant 1.25$ m and tends to locate around a geometric cone at larger propagation distances.

The percentage error of the energy given by Eq. (12) was computed for each propagation step of the Bessel–Gauss beam and is depicted in Fig. 2(d). Integration over the radial coordinate was performed with a simple trapezoidal rule. Notice that excellent results were obtained for the cylindrical coordinates approach and their superiority over the Cartesian coordinates method, Fig. 1(d). This difference emphasizes the higher performance of one-step propagation over the alternating direction implicit method and demonstrates how the percentage error can be used as a parameter to monitor the method's stability. In Fig. 2(d) we also show (dashed curve) the percentage error of the energy obtained on propagating the Bessel–Gauss beam using the quasi-discrete Hankel transform algorithm (see Ref. 11) with a super-Gaussian absorbing boundary.

6. CONCLUSION

We have extended the boundaryless one-dimensional propagation scheme of Ladouceur to two dimensions in Cartesian and cylindrical coordinates. This formulation is suitable for the scalar regime and can straightforwardly account for three-dimensional variations of the refraction index. The coordinate-mapping technique is used to avoid the assumption of artificial boundaries without any loss of field information, as occurs in the absorbing window or transparent boundary approach.[2,3] Keeping the field energy within the computational window is crucial to monitor energy preservation and ensure proper algorithm function.

Additionally, we have found and applied a field scaling factor that effectively simplifies the finite-difference equations in the Cartesian coordinate system. For the cylindrical coordinate formulation, the field scaling factor that eliminates the first derivative of the field with respect to the transverse radial coordinate proved to compromise numerical stability and is not implemented.

The proposed method is suitable for optical wave fields that are reasonably confined to the central region. Although the implemented numerical examples are not particularly suitable for this formulation, very good agreement was obtained from the comparison of their results and those of the analytical propagation solutions. This further confirms the method's robustness under appropriate adjustment of parameters.

The inherent limitations of the method, owing to insufficiently frequent sampling, were analyzed for band-limited wave fields. This clearly imposes a transverse limit in the physical space for accurate signal representation and further emphasizes the importance of careful adjustment of transformation scaling parameters.

We believe that this formulation will prove to be particularly useful to simulate propagation through longitudinally dependent waveguides with large variations in the transverse refraction index profile, since it is particularly suitable for modelike functions where most of the energy is located around the z axis. The fact that the field energy is always preserved inside the computational window with this method, unlike the absorbing or transparent boundary approach, provides a valuable control parameter to ensure the simulation accuracy.

ACKNOWLEDGMENTS

We acknowledge the fruitful comments of the referees that have helped us to improve the present manuscript. This work was supported by Consejo Nacional de Ciencia y Tecnología of México under grant 42808 and by the Tecnológico de Monterrey Research Chair in Optics under grant CAT-007.

Corresponding author Julio C. Gutiérrez-Vega can be reached by e-mail at juliocesar@itesm.mx.

REFERENCES

1. M. D. Feit and J. A. Fleck, "Light propagation in graded-index optical fibers," Appl. Opt. **17**, 3990–3998 (1978).
2. G. Mur, "Absorbing boundary conditions for finite-difference approximation of the time-domain electromagnetic field equations," IEEE Trans. Electromagn. Compat. **23**, 377–382 (1981).
3. G. R. Hadley, "Transparent boundary condition for beam propagation," Opt. Lett. **16**, 624–626 (1991).
4. Y. Arai, A. Maruta, and M. Matsuhara, "Transparent

boundary for the finite-element beam-propagation method," Opt. Lett. **18**, 765–767 (1993).
5. F. Ladouceur, "Boundaryless beam propagation," Opt. Lett. **21**, 4–5 (1996).
6. J. Shibayama, K. Matsubara, M. Sekiguchi, J. Yamauchi, and H. Nakano, "Efficient nonuniform schemes for paraxial and wide-angle finite-difference beam propagation methods," J. Lightwave Technol. **17**, 677–683 (1999).
7. S. J. Hewlett and F. Ladouceur, "Fourier decomposition method applied to mapped infinite domains: scalar analysis of dielectric waveguides down to modal cutoff," J. Lightwave Technol. **13**, 375–383 (1995).
8. K. M. Lo and E. H. Li, "Solutions of the quasi-vector wave equation for optical waveguides in a mapped infinite domains by the Galerkin's method," J. Lightwave Technol. **16**, 937–944 (1998).
9. C. Pozrikidis, *Numerical Computation in Science and Engineering* (Oxford U. Press, 1998).
10. J. C. Gutiérrez-Vega and M. A. Bandres, "Helmholtz–Gauss waves," J. Opt. Soc. Am. A **22**, 289–298 (2005).
11. M. Guizar-Sicairos and J. C. Gutiérrez-Vega, "Computation of quasi-discrete Hankel transforms of integer order for propagating optical wavefields," J. Opt. Soc. Am. A **21**, 53–58 (2004).